Investigation of the Age-Dependent Constitutive Relations of Mortar

Huang Hsing Pan[1] and George J. Weng[2]

Abstract: The stress-strain relation of cement binder is age-dependent and so is the behavior of mortar. In this study, we conducted a concurrent experimental and theoretical investigation into the effect of material age on the properties of both cement binder and mortar. First the stress-strain curves of the binder were measured over a wide range of aging time from 7 days to 18 months. Two types of binder—one with the cement paste alone and the other with the fly ash/cement combination—were chosen in the tests. The test results were simulated with a modified, age-dependent Burgers rheological model. Then measured were the stress-strain curves of the mortar that contains the same types of cement at three levels of aggregate volume concentrations: $c_1 = 29$, 38, and 49%. A micromechanics-based composite model making use of the secant-moduli was then introduced to predict the age-dependent behavior of mortar at various aging times and aggregate concentrations. Direct comparison between the measured data and the composite predictions is found to be in close agreement. It suggests that the proposed micromechanics model could be a viable approach to the estimate of age-dependent constitutive relations of mortar. **DOI: 10.1061/(ASCE)EM.1943-7889.0000323.**

CE Database subject headings: Stress strain relations; Cement; Aggregates; Mortars; Micromechanics.

Author keywords: Age-dependent stress-strain relations; Cement paste; Aggregates; Mortar; Micromechanics.

Introduction

It is widely recognized that an accurate constitutive description for the behavior of cement paste and concrete (or mortar) is critical to their safe and long-life operation. For this reason many constitutive models have been proposed in the past (Carreira and Chu 1985; Tsai 1988; Mander and Priestley 1998; Alexander and Milne 1995; Yip 1998; Du et al. 2010). Most of these models are phenomenological. Although useful in their own right, the influence of aggregate concentration on the concrete (or mortar) behavior cannot be explicitly accounted for in these approaches. To address the influence of aggregate concentrations, some micromechanics approaches have been introduced recently by Kuo et al. (2008), Scheiner and Hellmich (2009), Grassl and Pearce (2010), and Pan and Weng (2010). These studies have focused on the modulus of elasticity and aspect-ratio dependence of the stress-strain curves of mortar, creep and relaxation of concrete, influence of temperature on the thermal mismatch between aggregates and cement paste, and strain-rate sensitivity of mortar, respectively. The micromechanics approach has proven to be particularly useful to the prediction of concrete or mortar properties as the aggregate concentration changes.

In addition to the dependence of aggregate concentration, the properties of concrete (or mortar) are also known to be sensitive to the environment, such as temperature, moisture, and aging time. To address these issues, a significant effort has been directed. In particular, Di Luzio (2009) have adopted a Maxwell chain to model the behavior of uncracked concrete and used it to study the time-dependent cracking process; Zhang et al. (2009) have examined the moisture distribution in early age concrete; and Chen et al. (2010) have measured the triaxial compressive strength in water environments.

The focus in this study is on the influence of material age on the stress-strain relations of both the cement paste and mortar. The novel feature of this work is that it covers a rather wide range of aging time, from 7 days to one and a half years (18 months). It will also include a wide range of aggregate volume concentration, from 0 (cement paste itself) to 49%. The experimental tests will also include the peak stress and peak strain at each aging time and aggregate concentration. Most studies on the material age often focus on the early age properties, typically up to 28 days. For instance. in the creep test programs of Laplante (1993) and Atrushi (2003) [as cited by Scheiner and Hellmich (2009) in their model verifications], the material ages were 20 h, 27 h, 3 days, 7 days, and 28 days in the former and 1, 2, 3, 4, 6, and 8 days in the latter. In the study of cement hydration and the hydration effect on creep, shrinkage, and cracking by Schutter (2004), Mabrouk et al. (2004), and Pane and Hansen (2008), the material ages were from 2 to 800 h (approximately 1 month). If parts of the cement paste are replaced by pozzolanic materials (silica fume, slag, or fly ash), a longer aging time is required (typically 56 or 90 days) because of the late pozzolanic reaction. It is quite possible that the aging time of 28 (or 56 or 90) days may not have fully reached the steady-state without (or with) the pozzolanic replacement. Seen some limited tests covering the early to long-term age of hardened concrete have been seen, but the focus has been either on the modulus of elasticity or on the failure strength (Katz 1996; Al-Khaiat and Fattuhi 2001; Lopez et al. 2007), none on the stress-strain relations. Because the stress-strain relation is a vital component of the constitutive laws, we believe that there is an urgent need to provide such data. It is with this belief that this work has been carried out.

[1]Professor, Dept. of Civil Engineering, Kaohsiung Univ. of Applied Sciences, Kaohsiung 807, Taiwan. E-mail: pam@cc.kuas.edu.tw

[2]Professor, Dept. of Mechanical and Aerospace Engineering, Rutgers Univ., New Brunswick, NJ 08903 (corresponding author). E-mail: weng@jove.rutgers.edu

Note. This manuscript was submitted on November 24, 2010; approved on August 4, 2011; published online on August 6, 2011. Discussion period open until August 1, 2012; separate discussions must be submitted for individual papers. This paper is part of the ***Journal of Engineering Mechanics***, Vol. 138, No. 3, March 1, 2012. ©ASCE, ISSN 0733-9399/2012/3-297–306/$25.00.

In the following, experimental data is presented on the stress-strain relations of cement pastes, and then the data of mortar using the same pastes. To translate the observed behaviors into useful constitutive models, a composite model will also be devised that treats the cement paste as the matrix and the sand aggregates as spheroidal inclusions. The measured age-dependent data of the cement paste will be taken as the input and used to predict the age-dependent stress-strain relations of the mortar. The predicted results will be compared with the test data.

Experimental Investigation

Two types of cement binder and six mortars at three aggregate concentrations, each with nine material ages—7 days, 14 days, 28 days, 2 months, 3 months, 6 months, 9 months, 12 months and 18 months, have been tested. The cement binders used in mortar were the same as those tested individually, so that the properties of cement binder obtained in the first program could be used in the developed composite model for a direct comparison with the measured stress-strain curves of mortar obtained in the second program. The experimental setups are similar to those used in recent studies (Kuo et al. 2008; Pan and Weng 2010).

Cement is Portland type I. The first type of binder is the 100% cement paste with a 0.45 water-to-cement ratio (w/c), and the second one is a fly ash/cement binder with a 0.41 water-to-binder ratio (w/b), where fly ash/cement binder consists of 85% cement and 15% fly ash by weight, approximately. Fly ash was supplied by Hsinta thermal power plant (Taiwan) and is categorized as F-type. These two types are to be referred to as the C-group and FC-group, standing for cement and fly ash/cement, respectively. Mortar was made from these two types of binder with three aggregate volume concentrations, $c_1 = 0.29$, 0.38, and 0.49 (aggregates are referred to as phase 1 in the composite model, and the binder as phase 0, the matrix phase). The aggregate is the sand consisting of 99% quartz in accordance with C109 Ottawa standard sand. The particle size of the sand is approximately $0.7 \sim 1.0$ mm with a specific gravity of 2.65, and the shape is similar to a prolate inclusion with an average aspect-ratio (length-to-diameter ratio), $\alpha = 1.13$. A typical optical image is shown in Fig. 1. The elastic bulk and shear moduli of the sand are $\kappa_1 = 19.46$ GPa and $\mu_1 = 18.44$ GPa, respectively (Baalbaki et al. 1991). Table 1 is the mixture proportion of the C-group cementitious materials, and Table 2 is for the FC-group, in which c_1 is the volume fraction of aggregate. In both Tables, the materials at $c_1 = 0$, denoted as C0 and FC0, represent the associated binder itself without aggregates.

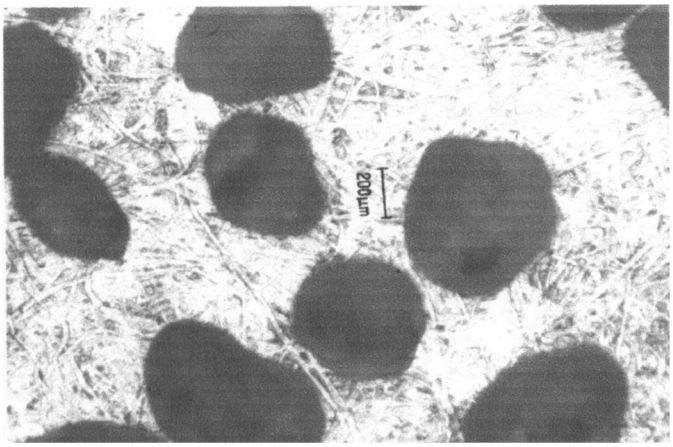

Fig. 1. Optical image of the aggregates

Table 1. Mixture Proportions (in kg) of Cement Paste Binder Composite (the *C*-Group)

Material	c_1	Water	Cement	Sand
C0	0	586	1302	—
C29	29%	415	921	775
C38	38%	362	804	1014
C49	49%	298	623	1301

Note: c_1 is the volume fraction of aggregates.

Table 2. Mixture Proportions (in kg) of Fly Ash/Cement Binder Composite (the FC-Group)

Material	c_1	Water	Cement	Fly ash	Sand
FC0	0	546	1133	200	—
FC29	29%	384	796	140	878
FC38	38%	334	693	123	1029
FC49	49%	275	570	101	1316

Note: c_1 is the volume fraction of aggregates.

(a)

(b)

Fig. 2. (a) an installation of extensometers for longitudinal and lateral strains; (b) a combination of shear and cleavage failure for C0 materials

Cylindrical specimens were prepared using steel molds with the size of $\phi 100 \times 200$ mm. The mold of the specimen was removed at 24 h of age after casting. All specimens were subjected to moist curing until the moment of testing. Six specimens of each material were tested, and a total of 864 specimens in Tables 1 and 2 were measured for the stress-strain relations. Each specimen was loaded under uniaxial compression by an MTS machine (a close-loop servohydraulic testing machine) with a constant strain-rate $\dot{\varepsilon} = 1 \times 10^{-5}/\text{s}$, until the specimen failed. Used were two extensometers located in the half height of a specimen with a ± 4 mm range to measure the longitudinal and lateral strains. Fig. 2(a) displays the installation of extensometers on the specimen parallel and perpendicular to the direction of applied load to record the longitudinal and lateral strains. Together with the applied stress, these data allowed plotting of the stress-strain curves and determination of the initial modulus of elasticity and Poisson's ratio of the binder and mortar at each material age.

Under a constant strain-rate, the specimens of cement binder and mortar fail with rapid brittle failure. The failure pattern of the specimen belongs to a combination of shearing and cleavage shown in Fig. 2(b). The specimen passing through the peak stress is very venerable to fast fragmentation, and it is hard to record the postpeak stress-strain data. Although the applied strain could be strictly controlled by a very small strain-rate on the test specimen to obtain the few postpeak data if the applied stress is near to and beyond the peak stress (Wee et al. 1996), the recorded descending stress-strain curve is very short because of the brittle nature of cementitious materials. Moreover, the nature of stress-strain relation of the descending portion is not the same as that of the ascending one because of possible cracking and different strain rates that set in. The descending part of the stress-strain curve becomes significant only when the mortar materials contain some fibers

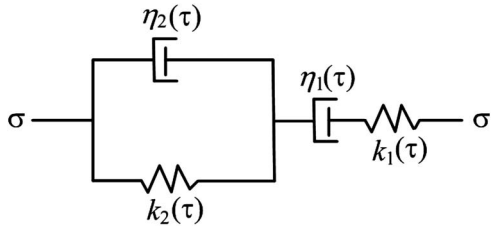

Fig. 3. A modified Burgers model for the age-dependent cement-based binder

in practical applications (Katz 1996; Nataraja et al. 1999). For these reasons, we only focus on the ascending branch of the stress-strain curve. We have also measured the maximum stress of the stress-strain curve (peak stress) and the strain corresponding to the maximum stress (peak strain); these data are given in Tables 3 and 4. The measured initial Young's modulus and Poisson's ratio are given in Tables 5 and 6. We shall use the modified Burgers model as depicted in Fig. 3 to represent the nonlinear viscoelastic behavior of the age-dependent cement paste.

The measured stress-strain curves of the C- and FC-group cement pastes at various aging times are shown in Figs. 4 and 5, respectively. The variations of peak stress and peak strain for both cement paste and mortar are given in Figs. 6–9, and the variations of initial Young's modulus are plotted in Figs. 10 and 11. Finally, the stress-strain curves of the mortar as the aggregate concentration increases from 0.29 to 0.38, and to 0.49, are depicted in Figs. 12–17. In Figs. 4, 5, and 12–17, it was observed that the stress-strain curves appear to reach a plateau before failure at the age of 7 days, and no plateau is found at 18 months. This is because cement hydration and pozzolanic reaction in cementitious binder have gradually developed with aging time according to the

Table 3. Peak Stress and Corresponding Strain for Cement Paste Binder Composite (the *C*-Group)

c_1	0%		29%		38%		49%	
Material age	stress (MPa)	strain (10^{-3})	stress (MPa)	strain (10^{-3})	stress (MPa)	strain (10^{-3})	stress (MPa)	strain (10^{-3})
7 days	42.31	6.81	43.42	4.54	43.97	4.33	44.05	4.28
14 days	44.85	6.66	46.07	4.44	47.68	4.21	48.57	4.13
28 days	48.23	6.22	49.80	4.22	52.25	4.15	52.90	4.09
2 months	51.74	5.93	54.01	4.12	55.92	3.98	56.41	3.94
3 months	53.32	5.51	56.14	4.10	58.15	3.95	58.74	3.88
6 months	54.45	5.48	57.04	3.98	59.07	3.78	60.01	3.79
9 months	54.89	5.30	57.78	3.81	59.85	3.70	61.14	3.66
12 months	55.25	5.20	58.34	3.77	60.57	3.63	61.43	3.62
18 months	55.30	5.13	58.80	3.77	61.29	3.63	61.93	3.61

Table 4. Peak Stress and Corresponding Strain for Fly Ash/Cement Binder Composite (the Fc-Group)

c_1	0%		29%		38%		49%	
Material age	stress (MPa)	strain (10^{-3})	stress (MPa)	strain (10^{-3})	stress (MPa)	strain (10^{-3})	stress (MPa)	strain (10^{-3})
7 days	45.91	6.43	47.51	4.40	49.03	4.26	49.21	4.06
14 days	48.97	6.21	50.79	4.22	52.61	4.13	53.70	4.01
28 days	52.22	5.95	54.42	4.08	56.81	4.04	57.35	3.91
2 months	55.79	5.64	57.90	4.01	60.34	3.92	61.40	3.82
3 months	57.15	5.51	60.05	3.93	62.69	3.85	63.86	33.74
6 months	58.26	5.26	61.10	3.88	63.55	3.72	64.75	3.59
9 months	58.45	5.12	61.59	3.83	64.13	3.69	65.24	3.51
12 months	58.85	4.96	62.14	3.79	64.52	3.60	65.92	3.49
18 months	59.02	4.86	62.41	3.77	65.20	3.53	66.46	3.45

Table 5. Young's Modulus (in Gpa) and Poisson's Ratio for Cement Paste Binder Composite (the C-Group)

c_1	0%		29%		38%		49%	
Material age	E	ν	E	ν	E	ν	E	ν
7 days	10.70	0.174	16.02	0.165	17.77	0.163	20.27	0.161
14 days	11.28	0.174	16.80	0.165	18.63	0.163	21.09	0.161
28 days	12.47	0.173	17.80	0.165	19.48	0.163	22.03	0.161
2 months	13.22	0.173	18.63	0.165	20.34	0.163	23.27	0.160
3 months	14.17	0.173	19.04	0.164	21.20	0.163	23.77	0.160
6 months	15.00	0.173	19.85	0.164	21.89	0.163	24.61	0.160
9 months	15.58	0.172	20.63	0.164	22.58	0.162	24.98	0.160
12 months	16.16	0.172	21.12	0.164	22.89	0.162	25.42	0.159
18 months	16.61	0.172	21.36	0.164	23.19	0.162	25.72	0.159

Table 6. Young's Modulus (in Gpa) and Poisson's Ratio for Fly Ash/Cement Binder Composite (the FC-Group)

c_1	0%		29%		38%		49%	
Material age	E	ν	E	ν	E	ν	E	ν
7 days	12.05	0.174	17.35	0.164	19.47	0.162	22.06	0.159
14 days	12.48	0.174	18.20	0.164	20.22	0.162	22.57	0.159
28 days	13.59	0.174	19.24	0.164	21.12	0.162	23.57	0.158
2 months	15.09	0.174	20.64	0.164	22.34	0.162	24.71	0.158
3 months	16.12	0.173	21.09	0.163	23.01	0.161	25.35	0.158
6 months	16.66	0.173	21.82	0.163	23.70	0.161	26.08	0.158
9 months	17.18	0.173	22.51	0.163	24.04	0.160	26.47	0.157
12 months	17.52	0.173	22.71	0.162	24.16	0.160	26.76	0.157
18 months	17.93	0.172	22.83	0.162	24.57	0.160	26.99	0.157

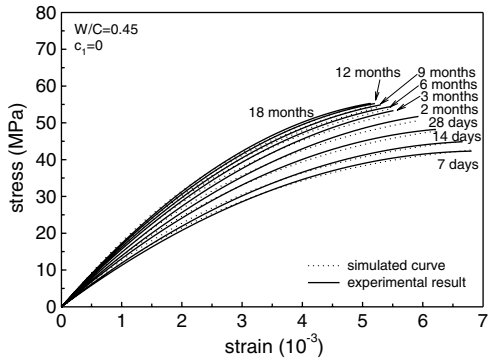

Fig. 4. Simulations and experiments for cement paste binders ($c_1 = 0$)

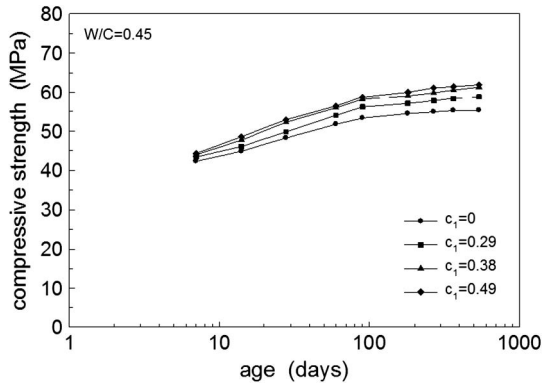

Fig. 6. Peak stress and material age for cement paste binder and mortar

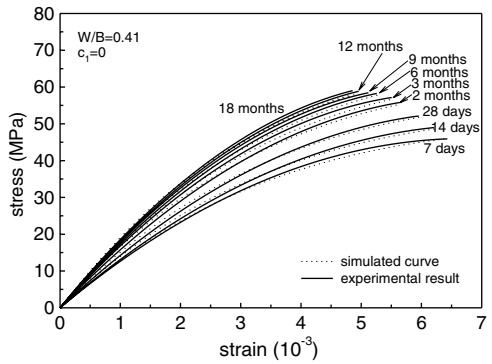

Fig. 5. Simulations and experiments for fly ash/cement binders ($c_1 = 0$)

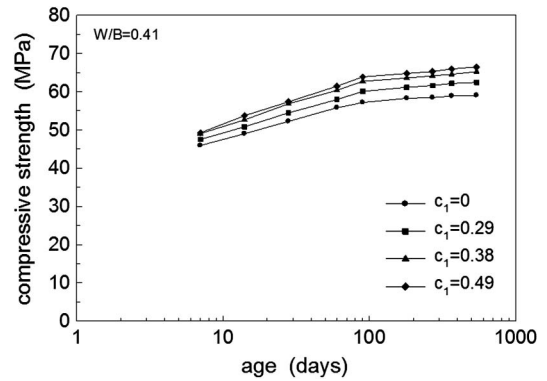

Fig. 7. Peak stress and material age for fly ash/cement binder and mortar

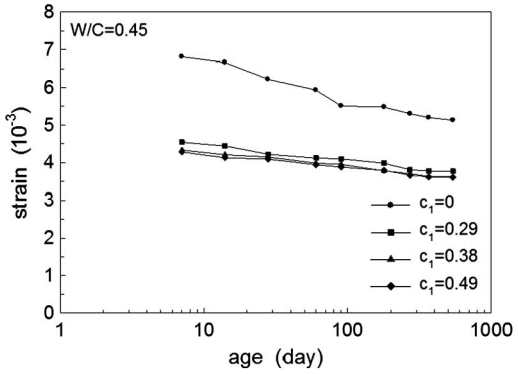

Fig. 8. Peak strain and material age for cement paste binder and mortar

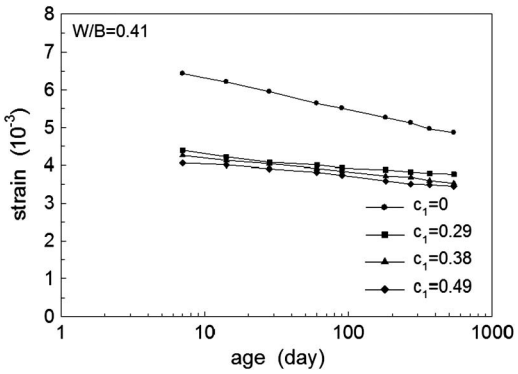

Fig. 9. Peak strain and material age for fly ash/cement binder and mortar

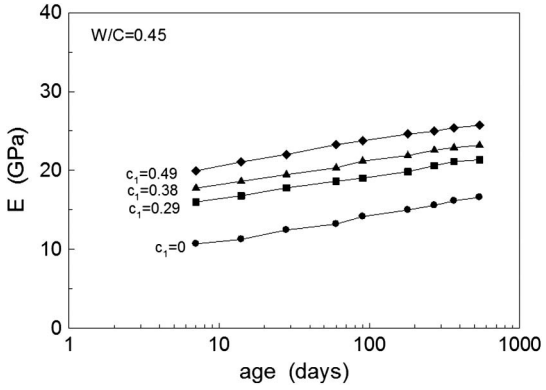

Fig. 10. Modulus of elasticity and material age for cement paste binder and mortar

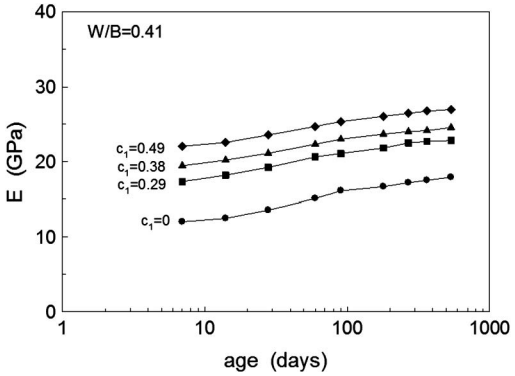

Fig. 11. Modulus of elasticity and material age for fly ash/cement binder and mortar

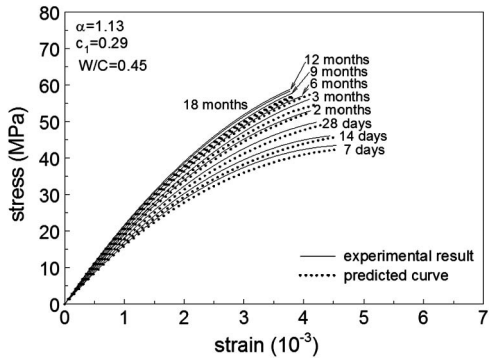

Fig. 12. Age-dependent stress-strain curves of C29 mortar

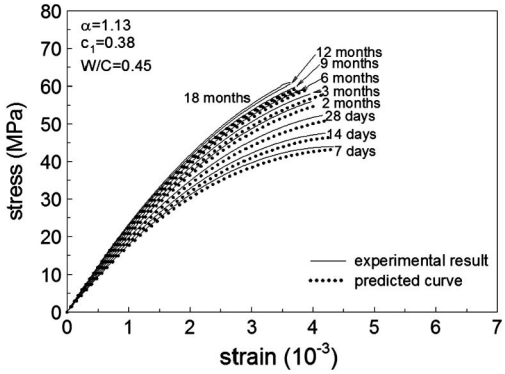

Fig. 13. Age-dependent stress-strain curves of C38 mortar

environmental circumstances, such as the moisture and temperature (Mehta 1986). More cement hydration and pozzolanic reaction will cause mortars to become stiffer and display more brittle behavior, and this leads to the increase of peak stress but the decrease of peak strain. These data will be revisited in the Results and Discussion.

Theoretical Modeling

An age-dependent Burgers model is first presented to simulate the measured stress-strain curves of the cement paste, and then a micromechanics-based composite model is introduced to predict the age-dependent stress-strain behavior of the mortar at several aggregate volume concentrations.

Age-Dependent Burgers Model for the Cement Paste

The experimental stress-strain curves of both C- and FC-group binders behave nonlinearly but display a steady-state at larger strain. To model this nonlinearity, we have found that the 4-parameter Burgers rheological model with age-dependent material constants could adequately describe the observed behavior. Such a model is depicted in Fig. 3, in which the spring constants and viscosities are represented by $k_1(\tau)$, $k_2(\tau)$, $\eta_1(\tau)$, and $\eta_2(\tau)$,

respectively, where τ is the aging time. The governing differential equation for this Burgers model is

$$\ddot{\sigma} + \left(\frac{k_1(\tau)}{\eta_1(\tau)} + \frac{k_1(\tau)}{\eta_2(\tau)} + \frac{k_2(\tau)}{\eta_2(\tau)}\right)\dot{\sigma} + \frac{k_1(\tau)\cdot k_2(\tau)}{\eta_1(\tau)\cdot\eta_2(\tau)}\sigma = \frac{k_1(\tau)\cdot k_2(\tau)}{\eta_2(\tau)}\dot{\varepsilon} + k_1(\tau)\ddot{\varepsilon}, \quad (1)$$

where σ = stress; ε = strain; and the dot above it indicates the time derivative. These experiments have been carried out under a constant strain-rate loading, so $\dot{\varepsilon} = \text{const} \equiv w$, and $\ddot{\varepsilon} = 0$. The solution to this differential equation carries a homogeneous and a particular one of the type $\sigma(t) = be^{mt} + ae^{nt} + \eta_1 w$, in which m and n are the characteristic roots of the homogeneous solution, given by:

$$m = \frac{\sqrt{\{k_1(\tau)\eta_2(\tau) + [k_1(\tau) - k_2(\tau)]\eta_1(\tau)\}^2 + 4k_1(\tau)k_2(\tau)\eta_1^2(\tau)} - k_1(\tau)\eta_2(\tau) - [k_1(\tau) + k_2(\tau)]\eta_1(\tau)}{2\eta_1(\tau)\eta_2(\tau)}$$
$$n = \frac{\sqrt{\{k_1(\tau)\eta_2(\tau) + [k_1(\tau) - k_2(\tau)]\eta_1(\tau)\}^2 + 4k_1(\tau)k_2(\tau)\eta_1^2(\tau)} + k_1(\tau)\eta_2(\tau) + [k_1(\tau) + k_2(\tau)]\eta_1(\tau)}{2\eta_1(\tau)\eta_2(\tau)} \quad (2)$$

The initial condition that $\sigma(0) = 0$ gives $a = -(b + \eta_1 w)$, leading to

$$\sigma(t) = b\left[e^{mt} - \left(\frac{n_1(\tau)w + b}{b}\right)\cdot e^{nt}\right] + \eta_1(\tau)w. \quad (3)$$

Because the strain is given by $\varepsilon = wt$, the dependence of stress on strain can be established by replacing t by ε/w, as

$$\sigma(\varepsilon) = b\left[e^{m\varepsilon/w} - \left(\frac{\eta_1(\tau)w + b}{b}\right)\cdot e^{n\varepsilon/w}\right] + \eta_1(\tau)w. \quad (4)$$

Constant b is related to the Young's modulus E through the initial slope of the stress-strain curve. Taking the derivative of σ with respect to ε, it readily gives $b = (E + \eta_1 n)w/(m - n)$. Eq. (4) represents the constitutive equation of the cement paste binder.

The measured stress-strain curves in Fig. 4 and 5 were used for the C0- and the FC0-group to calibrate the material constants in the rheological model. For the C0-group, the following is arrived at:

$$k_1(\tau) = 0.05(\log\tau)^2 - 0.10(\log\tau) + 0.78$$
$$k_2(\tau) = 0.02(\log\tau)^2 - 10.5(\log\tau) + 12.5$$
$$\eta_1(\tau) = 0.13(\log\tau)^2 - 0.23(\log\tau) + 4.92$$
$$\eta_2(\tau) = -3.14(\log\tau)^2 - 5.51(\log\tau) + 153 \quad (5)$$

and for the FC0-group

$$k_1(\tau) = 0.04(\log\tau)^2 - 0.09(\log\tau) + 0.77$$
$$k_2(\tau) = 0.20(\log\tau)^2 - 1.53(\log\tau) + 12.4$$
$$\eta_1(\tau) = 0.11(\log\tau)^2 + 0.17(\log\tau) + 4.90$$
$$\eta_2(\tau) = -2.80(\log\tau)^2 - 4.47(\log\tau) + 148 \quad (6)$$

where k is in the unit of GPa; η in GPa·s; and τ in days. With these calibrated parameters the simulated stress-strain curves are shown in Figs. 4 and 5 in dotted lines. Although, in principle the stress-strain curves can be plotted with continuous strains without limitations, the results are meaningful only up to the peak stress because of the brittle characteristic. Comparison between the solid and dotted lines in both figures suggests that this set of constitutive equations could well represent the measured properties of the cement pastes (binder). With these age-dependent constants, Eq. (4) provides the σ versus ε relation of the binder that will serve as an input in the composite model.

Composite Model for the Mortar

As the binder and cement-based composite are under monotonically increasing load, the nonlinear stress-strain curves of the mortar at a given aging time and volume concentration of aggregates

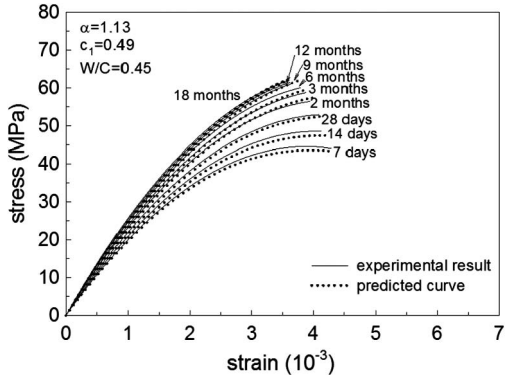

Fig. 14. Age-dependent stress-strain curves of C49 mortar

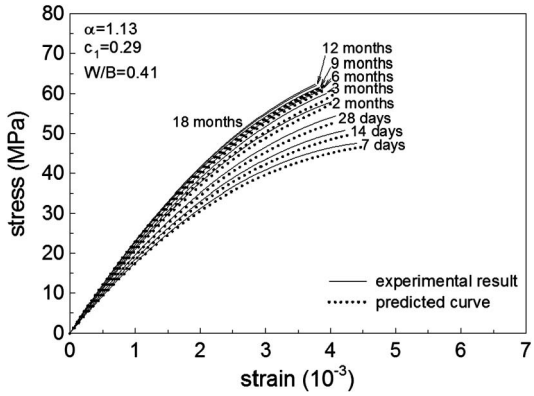

Fig. 15. Age-dependent stress-strain curves of FC29 mortar

can be conveniently calculated by using the secant-moduli approach. This approach constitutes a continuous replacement of the elastic moduli of the binder by its secant-moduli in the nonlinear range. This concept has previously been adopted to study the plasticity of particle-reinforced metal-matrix composites (Tandon and Weng 1988) and the transient and steady-state creep of metal-matrix composites (Pan and Weng 1993).

In this composite, the sand aggregates will be referred to as phase 1 and the cement binder as phase 0. The sand aggregates and cement binder are assumed to be perfectly bonded. The volume concentration of the rth phase is denoted by c_r and its bulk and shear moduli by k_r and μ_r, respectively. To apply the secant-moduli approach, its elastic counterpart must be introduced first. This can be accomplished through Eshelby's inclusion theory (1957) and Mori-Tanaka's average stress method (1973). The basic ingredients of the derivation involve: 1) first embed a single ellipsoidal inclusion in the matrix to calculate its strain (or stress) concentration tensor on the basis of Eshelby's solution, (2) take the volume average of the strains (or stresses) of the inclusions and the matrix, and set it equal to that of the composite to find the strain (or stress) concentration tensor of the matrix regarding the composite, and finally 3) use Hill's (1963) averaging principle to calculate the effective moduli of the composite. Detailed theoretical exposition can be found in Weng (1984, 1990) and Benveniste (1987). On the basis of this approach, the effective elastic bulk and shear moduli of the two-phase composite containing randomly oriented spheroidal inclusions can be written as (Tandon and Weng 1986)

$$\kappa = \frac{\kappa_0}{1 + c_1(p_2/p_1)}, \qquad \mu = \frac{\mu_0}{1 + c_1(q_2/q_1)}, \tag{7}$$

where

$$p_1 = 1 + c_1[2(S_{1122} + S_{2222} + S_{2233} - 1)(a_3 + a_4) + (S_{1111} + 2S_{2211} - 1)(a_1 - 2a_2)]/3a, \qquad p_2 = [a_1 - 2(a_2 - a_3 - a_4)]/3a,$$

$$q_1 = 1 - c_1\left\{\frac{2}{5}\frac{2S_{1212} - 1}{2S_{1212} + \mu_0/(\mu_1 - \mu_0)} + \frac{1}{3}\frac{2S_{2323} - 1}{2S_{2323} + \mu_0/(\mu_1 - \mu_0)} - \frac{1}{15a}[(S_{1122} - S_{2233})(2a_3 - a_4 + a_5 a) + 2(S_{1111} - S_{2211} - 1)(a_1 + a_2)]\right.$$
$$\left. + (S_{1122} - S_{2222} + 1)(2a_3 - a_4 - a_5 a)]\right\},$$

$$q_2 = -\frac{2}{5}\frac{1}{2S_{1212} + \mu_0/(\mu_1 - \mu_0)} - \frac{1}{3}\frac{1}{2S_{2323} + \mu_0/(\mu_1 - \mu_0)} + \frac{1}{15a}[2(a_1 + a_2 - a_3) + a_4 + a_5 a] \tag{8}$$

Constants a_1, a_2, a_3, a_4, a_5, and a depend on the shape of the aggregates as represented by Eshelby's S-tensor and the constituent moduli; these quantities are listed in the Appendix. When the shape is spherical, it reduces to (Weng 1984):

$$\kappa = \kappa_0\left[1 + \frac{c_1(\kappa_1 - \kappa_0)}{c_0\alpha_0(\kappa_1 - \kappa_0) + \kappa_0}\right], \qquad \mu = \mu_0\left[1 + \frac{c_1(\mu_1 - \mu_0)}{c_0\beta_0(\mu_1 - \mu_0) + \mu_0}\right] \tag{9}$$

where, regarding Poisson's ratio of the matrix, ν_0:

$$\alpha_0 = \frac{(1 + \nu_0)}{3(1 - \nu_0)}, \qquad \beta_0 = \frac{2(4 - 5\nu_0)}{15(1 - \nu_0)} \tag{10}$$

The aggregates will be taken to deform only elastically. For inclusions with a general ellipsoidal shape, the bulk and shear moduli of the isotropic composite can be found in Pan and Weng (1995).

The secant-moduli approach requires κ_0 and μ_0, and parameters p_1, p_2, q_1, and q_2 to be replaced by their corresponding secant-moduli at a given strain ε and aging time, τ. That is, κ_0 and μ_0 of the matrix phase in Eqs. (7) and (8) need to be replaced by its secant-moduli, $\kappa_0^s(\varepsilon, \tau)$, and $\mu_0^s(\varepsilon, \tau)$, which are related to the secant Young's modulus E_0^s by $\kappa_0^s = E_0^s/3(1 - 2\nu_0)$ and $\mu_0^s = E_0^s/2(1 + \nu_0)$. The value of E_0^s at a given level of strain can be calculated from Eq. (4) through $E_0^s = \sigma(\epsilon)/\epsilon$, and the Poisson ratio ν_0 is assumed to remain constant. In this way, the effective secant bulk and shear moduli of the composite follow from

$$\kappa_s(\varepsilon, \tau) = \frac{\kappa_0^s(\varepsilon, \tau)}{1 + c_1[p_2(\varepsilon, \tau)/p_1(\varepsilon, \tau)]}, \qquad \mu_s(\varepsilon, \tau) = \frac{\mu_0^s(\varepsilon, \tau)}{1 + c_1[q_2(\varepsilon, \tau)/q_1(\varepsilon, \tau)]} \tag{11}$$

Here, the secant-moduli of the binder are related to its secant Young's modulus E_0^s through

$$\kappa_0^s(\varepsilon, \tau) = \frac{E_0^s(\varepsilon, \tau)}{3(1 - 2\nu_0)}, \qquad \mu_0^s(\varepsilon, \tau) = \frac{E_0^s(\varepsilon, \tau)}{2(1 + \nu_0)} \tag{12}$$

Once $\kappa_s(\varepsilon, \tau)$ and $\mu_s(\varepsilon, \tau)$ of the composite are known, its secant Young modulus $E_s(\varepsilon, \tau)$ can be evaluated from

$$E_s(\varepsilon, \tau) = \frac{9\kappa_s(\varepsilon, \tau)\mu_s(\varepsilon, \tau)}{3\kappa_s(\varepsilon, \tau) + \mu_s(\varepsilon, \tau)} \tag{13}$$

The nonlinear stress-strain relation of the mortar then can be computed from this composite model at a given aggregate concentration c_1, aspect-ratio α, and aging time τ.

Even though this model can, in principle, be used to calculate the stress-strain curves of the mortar at any given aggregate concentration, it is suggested that it should never go beyond

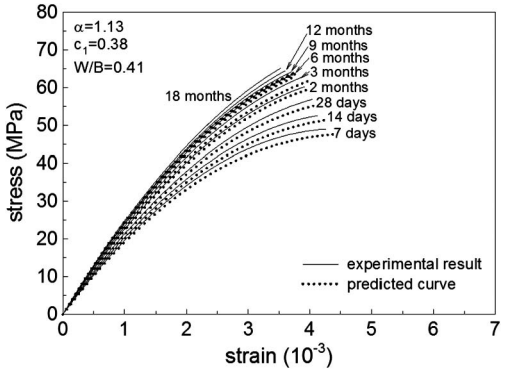

Fig. 16. Age-dependent stress-strain curves of FC38 mortar

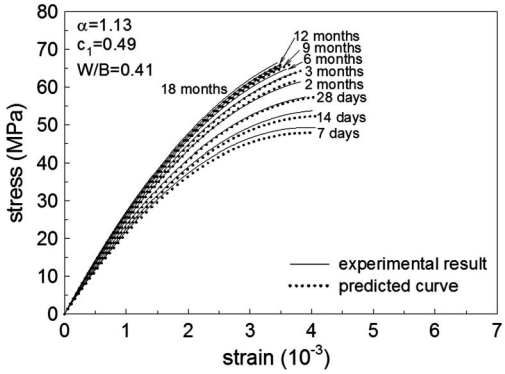

Fig. 17. Age-dependent stress-strain curves of FC49 mortar

50%. A previous study (Kuo et al. 2008) indicated that, at 60%, the aggregates are not fully bonded to the matrix. Furthermore, the strain range should be limited to the ascending branch of the stress-strain curve before microcracks develop. Once the stress-strain curve passes through the peak stress, sand aggregates are not well-bonded with the cement binder, and the model will no longer be suitable for applications.

Results and Discussion

Before proceeding to the calculated composite results, the measured peak stress and peak strain, and the modulus of elasticity will first be examined. It is to be noted that each reported data point is the averaged value over at least six specimens.

Age-Dependent Peak Stress and Peak Strain, and Modulus of Elasticity

The peak stresses for the moist-cured C-group materials have already been shown in Table 3 and plotted in Fig. 6. It is seen that the compressive strength increases with the material age, but the increasing rate tends to decrease if the material ages are more than 3 months. This threshold age is commonly observed if mortar is moist-cured, but is known to be a bit shorter if cured in air (Mehta 1986). The peak stress of the mortar at $c_1 = 0.49$ also increases with age, but the peak stresses are close to those with $c_1 = 0.38$ at each age. It appears that, for mortar with fine sand ($0.7 \sim 1.0$ mm), the increase of peak stress beyond $c_1 = 0.38$ is inefficient because at $c_1 = 0.49$ the binder could no longer bind up the sand particles completely. The peak stresses for the FC-group materials have also been given in Table 4 and plotted in Fig. 7. The threshold age for the compressive strength increase is also approximately 3 months because of the late pozzolanic reaction (adding fly ash) and moist curing. The displayed trends are similar to those of the C-group.

The axial strain at the peak stress is directly measured from the extensometer in Fig. 2. This approach is different from Yi et al. (2003) who adopted the platen-to-platen displacement of the specimen (where peak strain at 28 days was larger with a higher strength level compared with the early ages). The peak strains with aging time shown in Tables 3 and 4 are depicted in Figs. 8 and 9, respectively. Harsh et al. (1990) also indicated that the lower the sand content, the higher the strain at the peak stress. From Figs. 8 and 9, it is observed that the peak strain of all materials tends to decrease with aging time, and that the binder phase ($c_1 = 0$) has the greatest value of peak strain at each age. For instance, the peak strain of the C0 material shown in Table 3 decreases from 6.81×10^{-3} to 5.13×10^{-3} as the aging time increases from 7 days to 18 months, and at $c_1 = 0.49$ it decreases from 4.28×10^{-3} to 3.61×10^{-3}. The peak strain of FC0 shown in Table 4 decreases from 6.43×10^{-3} to 4.86×10^{-3} and, at $c_1 = 0.49$ it decreases from 4.06×10^{-3} to 3.45×10^{-3} during the same period of aging time. Material age is seen to have a very strong effect on both peak stress and peak strain, but the aggregate concentration also plays a key role. When c_1 increases from 0.29 to 0.49, the peak strain also decreases at each material age.

The elastic Young's modulus E and Poisson's ratio ν of the C-group and FC-group materials have been calculated from the initial axial and lateral response of the stress-strain relations; the results are given in Tables 5 and 6, respectively, following the ASTM C469 guidline. The Poisson ratios for all materials are seen to remain relatively constant as the material age increases. Figs. 10 and 11 show such dependence for E. It is evident that both material age and aggregate concentration have a strong effect on the stiffness of mortar.

Also noted is that fly ash, categorized as a kind of pozzolanic material, usually acts as a partial replacement of cement in mortar. Fly ash added into cement needs alkali (supplied by cement hydration) to create the so-called pozzolanic reaction whose products provide more efficient filling to large capillary space, thus, improving the strength, impermeability, and durability of the mortar materials (Mehta 1986). Comparing these two groups, it is found that the fly ash/cement group (the FC-group) has a higher peak stress and higher modulus of elasticity than the pure cement group (the C-group) in each category. The increase is approximately 8% for the peak stress and can be as high as 20% for the modulus of elasticity with the short aging time of 7 days, but as the material age increases to 18 months, the difference between the two narrows considerably.

Age-Dependent Stress-Strain Relations of the Mortar

On the basis of the composite model, the stress-strain curves of the mortar with the aggregate concentrations of $c_1 = 0.29$, 0.38, and 0.49 were calculated, all at the aspect-ratio of $\alpha = 1.13$. In each case, nine aging times ranging from 7 days to 18 months has been considered. Both the experimental and predicted results are shown in Figs. 12–14 for the C-group mortar and in Figs. 15–17 for the FC-group.

The predicted results follow the general trends of the measured curves closely. It is believed that that the slightly lower theoretical curves could be attributed to the lower simulated curves for the cement binders shown in earlier Figs. 4 and 5, but no need exists to recalibrate those earlier simulations because they are sufficiently close to the test data. So, the slightly lower theoretical estimates—which involve no adjustable parameters—are not caused by the

composite model itself. Overall, the agreement with the test data extends into a significant range of strain and covers the entire span of aging time and aggregate concentration.

From this comparison, it is concluded that the developed composite model, in conjunction with the age-dependent Burgers model, can be applied with sufficient accuracy to predict the age-dependent stress-strain relations of the mortar.

Conclusions

In this work, a coordinated experimental and theoretical investigation was conducted on the stress-strain relations of cement binder and mortar as a function of material age. The stress-strain curves of two types of cement binder were first measured, one without and the other with the fly ash content, and then the measured data was simulated with a modified, age-dependent Burgers rheological model. The age-dependent Burgers rheological model can be used to simulate the age-dependent stress-strain curves of cementitious binders sufficiently well. Then measured were the stress-strain curves of the mortar that contained the same cement binders at three levels of aggregate concentrations. A micromechanics-based composite model was devised to predict the nonlinear stress-strain behavior of the composites. In all these studies, the material age covers the wide range of 7 days to 18 months and the aggregate concentration from 0 to 49%. On the basis of the developed composite model, the predicted stress-strain curves are found to be in close agreement with the test data regardless of the aggregate concentration and material age. The obtained data up to 18 months of aging time and 49% of aggregate concentrations are new, and the proposed micromechanics approach can be useful for future applications.

Appendix: Components of a_1, a_2, a_3, a_4, a_5, and a

These components were originally presented in Tandon and Weng (1986), as

$$
\begin{aligned}
a_1 &= 6(\kappa_1-\kappa_0)(\mu_1-\mu_0)(S_{2222}+S_{2233}-1)\\
&\quad -2(\kappa_0\mu_1-\kappa_1\mu_0)+6\kappa_1(\mu_1-\mu_0)\\
a_2 &= 6(\kappa_1-\kappa_0)(\mu_1-\mu_0)S_{1133}+2(\kappa_0\mu_1-\kappa_1\mu_0)\\
a_3 &= -6(\kappa_1-\kappa_0)(\mu_1-\mu_0)S_{3311}-2(\kappa_0\mu_1-\kappa_1\mu_0)\\
a_4 &= 6(\kappa_1-\kappa_0)(\mu_1-\mu_0)(S_{1111}-1)+2(\kappa_0\mu_1-\kappa_1\mu_0)\\
&\quad +6\mu_1(\kappa_1-\kappa_0)\\
a_5 &= 1/[S_{3322}-S_{3333}+1-\mu_1/(\mu_1-\mu_0)]\\
a &= 6(\kappa_1-\kappa_0)(\mu_1-\mu_0)[2S_{1133}S_{3311}-(S_{1111}-1)\\
&\quad \times(S_{3322}+S_{3333}-1)]+2(\kappa_0\mu_1-\kappa_1\mu_0)[2(S_{1133}+S_{3311})\\
&\quad +(S_{1111}-S_{3322}-S_{3333})]-6\kappa_1(\mu_1-\mu_0)(S_{1111}-1)\\
&\quad -6\mu_1(\kappa_1-\kappa_0)(S_{2222}+S_{2233}-1)-6\kappa_1\mu_1, \qquad (14)
\end{aligned}
$$

regarding Eshelby's S-tensor, where direction 1 is the symmetric axis of the spheroid. With spheroidal inclusions whose aspect-ratio (length-to-diameter ratio) is represented by α, the components of S_{ijkl} are (Mura 1987; Zhao et al. 1989):

$$
\begin{aligned}
S_{1111} &= \frac{1}{2(1-\nu_0)}\left\{1-2\nu_0+\frac{3\alpha^2-1}{\alpha^2-1}-\left[1-2\nu_0+\frac{3\alpha^2}{\alpha^2-1}\right]g\right\},\\
S_{2222} &= S_{3333}=\frac{3}{8(1-\nu_0)}\frac{\alpha^2}{\alpha^2-1}\\
&\quad +\frac{1}{4(1-\nu_0)}\left[1-2\nu_0-\frac{9}{4(\alpha^2-1)}\right]g,\\
S_{2233} &= S_{3322}=\frac{1}{4(1-\nu_0)}\left\{\frac{\alpha^2}{2(\alpha^2-1)}\right.\\
&\quad \left.-\left[1-2\nu_0+\frac{3}{4(\alpha^2-1)}\right]g\right\},\\
S_{2211} &= S_{3311}=-\frac{1}{2(1-\nu_0)}\frac{\alpha^2}{\alpha^2-1}\\
&\quad +\frac{1}{4(1-\nu_0)}\left[\frac{3\alpha^2}{\alpha^2-1}-(1-2\nu_0)\right]g,\\
S_{1122} &= S_{1133}=-\frac{1}{2(1-\nu_0)}\left[1-2\nu_0+\frac{1}{\alpha^2-1}\right]\\
&\quad +\frac{1}{2(1-\nu_0)}\left[1-2\nu_0+\frac{3}{2(\alpha^2-1)}\right]g,\\
S_{2323} &= \frac{1}{4(1-\nu_0)}\left\{\frac{\alpha^2}{2(\alpha^2-1)}+\left[1-2\nu_0-\frac{3}{4(\alpha^2-1)}\right]g\right\},\\
S_{1212} &= S_{1313}=-\frac{1}{4(1-\nu_0)}\left\{1-2\nu_0-\frac{\alpha^2+1}{\alpha^2-1}\right.\\
&\quad \left.-\frac{1}{2}\left[1-2\nu_0-\frac{3(\alpha^2+1)}{\alpha^2-1}\right]g\right\}, \qquad (15)
\end{aligned}
$$

where ν_0 is Poisson's ratio of the matrix, and function g depends on the aspect-ratio α as $g=\frac{\alpha}{(\alpha^2-1)^{3/2}}[\alpha(\alpha^2-1)^{1/2}-\cosh^{-1}\alpha]$ for prolate shape and

$$
g=\frac{\alpha}{(1-\alpha^2)^{3/2}}[\cos^{-1}\alpha-\alpha(1-\alpha^2)^{1/2}], \qquad \text{for oblate shape} \qquad (16)
$$

Acknowledgments

H. H. Pan was supported by the Taiwan National Science Council under NSC 93-2211-E-151-007, and G. J. Weng by the National Science Foundation under CMS 05-10409.

References

Alexander, M. G., and Milne, T. I. (1995). "Influence of cement blend and aggregate type on stress-strain behavior and elastic modulus of concrete." *ACI Mater. J.*, 92(3), 227–235.

Al-Khaiat, H., and Fattuhi, N. (2001). "Long-term strength development of mortar in arid conditions." *Cem. Concr. Compos.*, 23(4), 363–373.

Atrushi, D. (2003). "Tensile and compressive creep of early age concrete: testing and modeling." Ph.D. thesis, Norwegian Univ. of Science and Technology, Trondheim, Norway.

Baalbaki, W., Benmokkrane, B., Chaallal, O., and Aitcin, P. C. (1991). "Influence of coarse aggregate on elastic properties of high-performance concrete." *ACI Mater. J.*, 88(5), 499–503.

Benveniste, Y. (1987). "A new approach to the application of Mori-Tanaka theory in composite materials." *Mech. Mater.*, 6(2), 147–157.

Carreira, D. J., and Chu, K. H. (1985). "Stress-strain relationship for plain concrete in compression." *J. Am. Concr. Inst.*, 82(6), 797–804.

Chen, Z., Hu, Y., Li, Q. B., Sun, M. Y., Lu, P. Y., and Liu, T. Y. (2010). "Behavior of concrete in water subjected to dynamic triaxial compression." *J. Eng. Mech.*, 136(3), 379–389.

Di Luzio, G. (2009). "Numerical model for time-dependent fracturing of concrete." *J. Eng. Mech.*, 135(7), 632–640.
Du, X. L., Lu, D. C., Gong, Q. M., and Zhao, M. (2010). "Nonlinear unified strength criterion for concrete under three-dimensional stress states." *J. Eng. Mech.*, 136(1), 51–59.
Eshelby, J. D. (1957). "The determination of the elastic field of an ellipsoidal inclusion, and related Problems." *Proc., R. Soc. Lond., A*, 241(1226), 376–396.
Grassl, P., and Pearce, C. (2010). "Mesoscale approach to modeling concrete subjected to thermomechanical loading." *J. Eng. Mech.*, 136(3), 322–328.
Harsh, S., Shen, Z., and Darwin, D. (1990). "Strain-rate sensitive behavior of cement paste and mortar in compression." *ACI Mater. J.*, 87(5), 508–515.
Hill, R. (1963). "Elastic properties of reinforced solids: Some theoretical principles." *J. Mech. Phys. Solids*, 11(5), 357–372.
Katz, A. (1996). "Effect of fiber modulus of elasticity on the long term properties of micro-fiber reinforced cementitious composites." *Cem. Concr. Compos.*, 18(6), 389–399.
Kuo, T. H., Pan, H. H., and Weng, G. J. (2008). "Micromechanics-based predictions on the overall stress-strain relations of cement-matrix composites." *J. Eng. Mech.*, 134(12), 1045–1052.
Laplante, P. (1993). "Properties mecaniques de betons durcissants: Analyse comparee des betons classique et a tres hautes performances [Mechanical properties of hardening concrete: A comparative analysis of ordinary and high performance concretes]." Ph.D. thesis, Ecole Nationale des Ponts et Chaussees, Paris (in French).
Lopez, M., Kahn, L. F., and Kurtis, K. E. (2007). "Characterization of elastic and time-dependent deformation in normal strength and high performance concrete by image analysis." *Cem. Concr. Res.*, 37(8), 1265–1277.
Mabrouk, R., Ishida, T., and Maekawa, K. (2004). "A unified solidification model of hardening concrete composite for predicting the young age behavior of concrete." *Cem. Concr. Compos.*, 26(5), 453–461.
Mander, J. B., Priestley, M. J. N., and Park, R. (1988). "Theoretical stress-strain model for confined concrete." *J. Struct. Eng.*, 114(8), 1804–1826.
Mehta, P. K. (1986). *Mortar- structure, properties, and materials*, Prentice-Hall, NJ.
Mori, T., and Tanaka, K. (1973). "Average stress in matrix and average elastic energy of materials with misfitting inclusions." *Acta Metall.*, 21(5), 571–574.
Mura, T. (1987). *Micromechanics of defects in solids*, 2nd Ed., Martinus Nijhoff, Dordrecht, The Netherlands.
Nataraja, M. C., Dhang, N., and Gupta, A. P. (1999). "Stress-strain curves for steel-fiber reinforced concrete under compression." *Cem. Concr. Compos.*, 21(5), 383–390.
Pan, H. H., and Weng, G. J. (1993). "Determination of transient and steady-state creep of metal-matrix composites by a secant moduli method." *Compos. Eng.*, 3(7-8), 661–674.
Pan, H. H., and Weng, G. J. (1995). "Elastic moduli of heterogeneous solids with ellipsoidal inclusions and elliptic cracks." *Acta Mech.*, 110(1-4), 73–94.
Pan, H. H., and Weng, G. J. (2010). "Study on strain-rate sensitivity of cementitious composites." *J. Eng. Mech.*, 136(9), 1076–1082.
Pane, I., and Hansen, W. (2008). "Investigation on key properties controlling early-age stress development of blended cement concrete." *Cem. Concr. Res.*, 38(11), 1325–1335.
Scheiner, S., and Hellmich, C. (2009). "Continuum microviscoelasticity model for aging basic creep of early-age concrete." *J. Eng. Mech.*, 135(4), 307–323.
Schutter, G. D. (2004). "Applicability of degree of hydration concept and maturity method for thermo-visco-elastic behaviour of early age concrete." *Cem. Concr. Compos.*, 26(5), 437–443.
Tandon, G. P., and Weng, G. J. (1986). "Average stress in the matrix and effective moduli of randomly oriented composites." *Compos. Sci. Technol.*, 27(2), 111–132.
Tandon, G. P., and Weng, G. J. (1988). "A theory of particle-reinforced plasticity." *J. Appl. Mech.*, 55(1), 126–135.
Tsai, W. T. (1988). "Uniaxial compression at stress-strain relation of concrete." *J. Struct. Eng.*, 114(9), 2133–2136.
Wee, T. H., Chin, M. S., and Mansur, M. A. (1996). "Stress-strain relationship of high-strength concrete in compression." *J. Mater. Civ. Eng.*, 8(2), 70–76.
Weng, G. J. (1984). "Some elastic properties of reinforced solids, with special reference to isotropic ones containing spherical inclusions." *Int. J. Eng. Sci.*, 22(7), 845–856.
Weng, G. J. (1990). "The theoretical connection between Mori-Tanaka's theory and the Hashin-Shtrikman-Walpole bounds." *Int. J. Eng. Sci.*, 28(11), 1111–1120.
Yi, S. T., Kim, J. K., and Oh, T. K. (2003). "Effect of strength and age on the stress-strain curves of concrete specimens." *Cem. Concr. Res.*, 33(8), 1235–1244.
Yip, W. K. (1998). "Generic form of stress-strain equations for concrete." *Cem. Concr. Res.*, 28(4), 499–508.
Zhang, J., Qi, K., and Huang, Y. (2009). "Calculation of moisture distribution in early-age concrete." *J. Eng. Mech.*, 135(8), 871–880.
Zhao, Y. H., Tandon, G. P., and Weng, G. J. (1989). "Elastic moduli for a class of porous materials." *Acta Mech.*, 76(1-2), 105–130.